Effect of Cladding Direction on Residual Stress Distribution in Laser Cladded Rails

Taposh Roy, Anna Paradowska, Ralph Abrahams, Quan Lai, Michael Law, Peter Mutton, Mehdi Soodi, Wenyi Yan

Abstract—In this investigation, a laser cladding process with a powder feeding was used to deposit stainless steel 410L (high strength, excellent resistance to abrasion and corrosion, and great laser compatibility) onto railhead (higher strength, heat treated hypereutectoid rail grade manufactured in accordance with the requirements of European standard EN 13674 Part 1 for R400HT grade), to investigate the development and controllability of process-induced residual stress in the cladding, heat-affected zone (HAZ) and substrate and to analyse their correlation with hardness profile during two different laser cladding directions (across and along the track). Residual stresses were analysed by neutron diffraction at OPAL reactor, ANSTO. Neutron diffraction was carried out on the samples in longitudinal (parallel to the rail), transverse (perpendicular to the rail) and normal (through thickness) directions with high spatial resolution through the thickness. Due to the thick rail and thin cladding, 4 mm thick reference samples were prepared from every specimen by Electric Discharge Machining (EDM). Metallography across the laser claded sample revealed four distinct zones: The clad zone, the dilution zone, HAZ and the substrate. Compressive residual stresses were found in the clad zone and tensile residual stress in the dilution zone and HAZ. Laser cladding in longitudinally cladding induced higher tensile stress in the HAZ, whereas transversely cladding rail showed lower tensile behavior.

Keywords—Laser cladding, residual stress, neutron diffraction, HAZ.

I. INTRODUCTION

WEAR in the railhead is a common phenomenon in railway industries which cannot be avoided. Periodic repair or replacement of damaged/worn rails due to wear and/or fatigue cost a large portion of the total budget every year. Over the last decade, different alloys have been proposed and developed to prevent the damages of railway track. The limits of steel metallurgy and the complex nature of rolling contact fatigue require new solutions if track life is to be prolonged significantly. Previously, rail materials were made with a bainitic structure which exhibits high hardness [1] which was considered to increase the wear performances of rail materials [2]. However, the work hardening behaviour with pearlitic

structure has already been shown significant improvement wear and fatigue performances which ultimately prolonged the track life significantly in service [3], [4].

With increasing of axle loads, frequency, traction power and speed, rail failure and replacement are also increasing due to rolling contact fatigue (RCF) at the rail-wheel contact surface. RCF damage is generally caused by a combination of high cyclic normal and tangential stress between the rail and the wheel, resulting in the accumulation of plastic deformation (known as ratchetting) at the gauge corner. RCF defects show various forms, such as head checks, spalling, gauge corner cracks, and squashing [5]. Defects cause crack initiation either at the top surface (known as head checks) or subsurface cracks which propagate through the rail material, leading to spalling at the top surface and, in some cases, ultimately causing complete failure. In periodic maintenance, these defects can be detected and removed by grinding the rail top surface thus prolonging the life of the rail. So, protection of the rail top surface is very important. Laser cladding is an established metal deposition repairing/refabricating technique in tool and aerospace applications. One of its primary applications is the deposition of wear-resistant, fatigue-resistant and anti-corrosion coatings. In laser cladding, the melting process uses a laser beam to fuse an alloy addition onto a substrate which provides a full metallurgical bond, low heat input process and superior process control [6]. However, the addition of a clad layer results in the generation of residual stresses in the weld region due to several complex mechanisms. These include differences in thermal expansion between the clad layer and parent metals during cooling, thermal strains resulting from differences in heating/cooling at differing locations and the directional stiffness within the sections present.

In the last decade, significant progress has been achieved in the application of neutron diffraction to residual stress determination in rails [7]-[9]. To the authors' knowledge, all the residual stress measurement is limited to new and used rail [10] and the rail joint [11]. In this project, residual stresses in a clad surface were analysed by neutron diffraction at the OPAL reactor, ANSTO (Australian Nuclear Science and Technology Organisation). The effect of two laser cladding directions: along the rail (longitudinal direction) and across the rail (transverse direction) were analysed

II. EXPERIMENTAL PROCEDURE

A. Materials

Rail material was a head-hardened 68 kg/m rail. The laser clad material is a 410L grade stainless powder with 150 μm average particle diameter. Chemical compositions of the rail

Taposh Roy, Ralph Abrahams, Quan Lai, and Wenyi Yan are with Department of Mechanical and Aerospace Engineering, Monash University, Clayton VIC 3800, Australia (e-mail: taposh.roy@monash.edu, ralph.abrahams@monash.edu, quan.lai@monash.edu, wenyi.yan@monash.edu).

Anna Paradowska and Michael Law are with Australian Nuclear Science and Technology Organization, Lucas Heights 2234, NSW Australia (e-mail: anna.paradowska@ansto.gov.au, mlx@ansto.gov.au).

Peter Mutton is with Institute of Railway Technology, Monash University, Clayton VIC 3800, Australia (e-mail: peter.mutton@monash.edu).

Mehdi Soodi is with Hardchrome Engineering, Clayton VIC 3168, Australia (e-mail: mehdi@hardchrome.com.au).

World Academy of Science, Engineering and Technology
International Journal of Civil and Environmental Engineering
Vol:11, No:9, 2017

and cladding material are given in Table I. 410L laser clad material has been chosen for its high strength and excellent resistance to abrasion and corrosion.

TABLE I
CHEMICAL COMPOSITION OF VIRGIN RAIL AND CLAD 410L MATERIAL
(ELEMENTS ARE IN WEIGHT %)

Element	Virgin rail	410L	Element	Virgin rail	410L
Fe	-	Bal	Ni	<0.01	0.08
C	0.93	0.01	Mo	<0.01	0.01
Si	0.28	0.47	V	<0.01	0.01
Mn	0.95	0.51	Nb	<0.01	0.02
P	0.018	0.01	Al	<0.005	0.01
S	0.014	0.01	Ti	-	0.01
Cr	0.2	12.7	Cu	-	0.05

B. Laser Cladding

A schematic laser cladding process is illustrated in Fig. 1. Laser cladding was carried out with a laser coaxial head comprising of 4 kW IPG fibre laser gun and a Sultzer-Metco twin-10 powder feeder. The laser head was controlled by a Motoman XRC SK 16X 6-axis CNC unit. The laser beam was optically modified to deliver a concentrated circular laser spot of 5 mm on the surface of the substrate. An oxygen torch was used manually to preheat the sample to 350 °C before depositing the clad material on the rail. The laser cladding parameters were kept constant at 3.2 kW laser power; 1000 mm/s scanning speed; 26.4 g/min powder feed rate and 5 mm spot size. Shielding gas of 50% argon and 50% helium around the laser beam was used to avoid oxidation during the process. The cladded rail was cooled in open air to room temperature. More details of laser cladding were described in [12].

A 500 mm long rail piece was cladded, with the cladding length and width, 400 mm and 70 mm, respectively. These dimensions were based on typical in-situ rail repairs. The rail was cladded in two directions (Fig. 2): Along the rail (longitudinal direction) and across the rail (transverse direction) while other laser cladding parameters were kept constant.
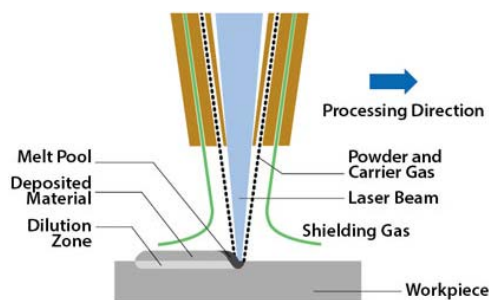

Fig. 1 Schematic diagram of laser cladding process [15]

Specimens were characterised for microstructure and hardness evaluation. Optical microscopy with image analysis was used for microstructure observation. A Kalling's no. 2 (5 g CuCl$_2$, 100 ml HCl and 100 ml ethanol) was used to visualise microstructure of the clad material. Microhardness was measured using the Struers A300 Duramin hardness tester. Micro-hardness measurements were taken at rail-cross

sections through thickness to investigate the hardness variation of different clad profile zone (clad layer, HAZ and substrate zone). Indentations of 5 kg-f were conducted vertically from the top surface of cladding to the unaffected base material. To mitigate errors caused by the "shallowing" effect (release of elastic stresses) and the distance between each indentation was approximately three times of the indenter's radius (~150 μm).
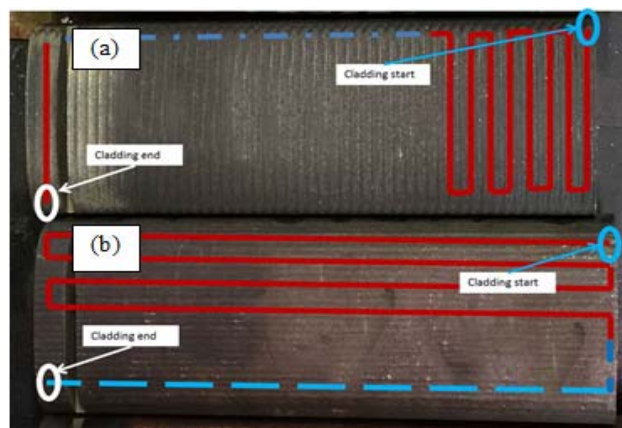

Fig. 2 Schematic diagram of laser cladding direction used in this experiment, (a) across the railhead (transverse direction); (b) along the rail head (longitudinal direction)
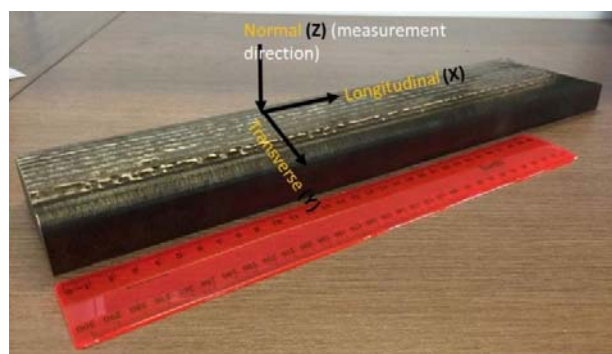

Fig. 3 Laser cladded sample showing the stress component and measurement direction

C. Residual Stress Measurement Procedure

The residual stress line scans through the thickness of the railheads were measured using the KOWARI Strain Scanner. The samples were aligned using SSCANSS software, KOWARI virtual instrument was used to optimize the measurements in distorted specimens. Fig. 3 shows the stress component and a measurement direction of rail sample.

For the strain measurements, reflection from α-Fe (211) plane has been used. The neutron wavelength of 1.67 Å was used at the detector angle, 2θ, of approximately 90° to ensure the cube shape of the gauge volume. A nominal gauge volume of $0.5 \times 0.5 \times 10$ mm^3 was used for all three components of strain.

The dimensions of the rails used in the experiment were 300 mm (length) × 70 mm (width) × 50 mm (thickness). The stress-free d_0 samples were fabricated using EDM machine from both control substrate rail and cladded rail.

World Academy of Science, Engineering and Technology
International Journal of Civil and Environmental Engineering
Vol:11, No:9, 2017

Line scans through the thickness of the stress-free d_0 samples were measured to find the position dependent reference value for residual stress calculation. The longitudinal, transverse and normal components of the residual stress field were calculated for each position in rail through thickness from the relevant three strain components. In the stress calculation, Young's modulus of 238 GPa and Poisson's ratio of 0.28 was used.

III. RESULTS AND DISCUSSIONS

A. Microstructure and Hardness

Figs. 4 (a) and (b) show the optical micrographs of transverse and longitudinal deposited clad layers respectively. The microstructure of as cladded martensitic stainless steel mainly consists of martensite, ferrite, un-dissolved carbide as well as retained austenite; the microstructure depends on the heat input and cooling rate during the cladding process [13], [14]. A fine dendritic microstructure was found in the transversely deposited clad layer in Fig. 4 (a). Formation of the dendritic microstructure can be described as the fast heat transfer from the clad layer to the substrate surface which acts as a massive heat sink. Inside the dendritic arms, martensite and retained austenite were reported. The change of cladding direction changed the morphology and microstructure of the clad layer (Fig. 4 (b)). The previous dendritic morphology was replaced by a granular morphology. Ferrite and retained austenite were identified in the optical micrograph as shown in Fig. 4 (b). Ferrite phase was most dominant in the clad layer of the longitudinally deposited cladding. More details about the microstructure can be found in a recently published paper from our group [12].
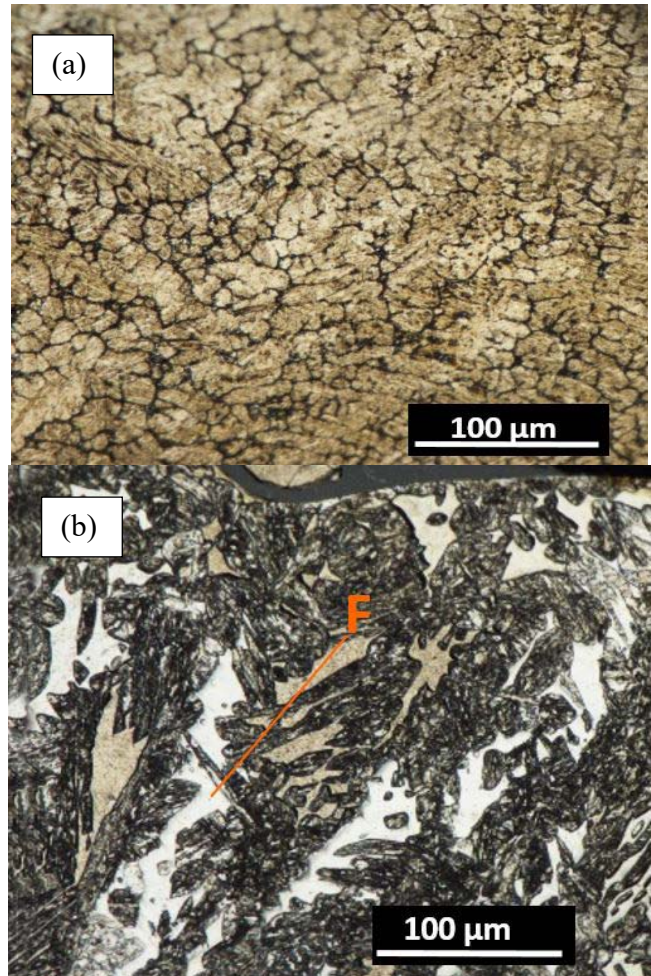

Fig. 4 Microstructure of clad area, (a) transversely deposited; (b) longitudinally deposited clad material
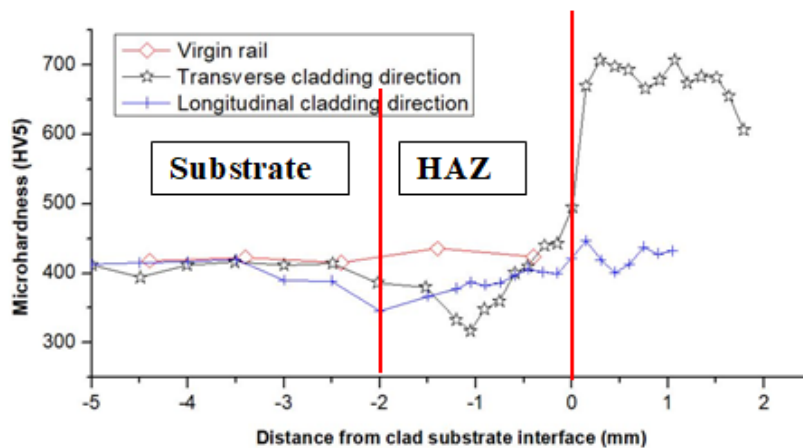

Fig. 5 Hardness variations in rail samples of virgin, longitudinally cladding and transversely cladding rail: X=0 represents the cladding-substrate interface

The hardness variation of railhead through the thickness is shown in Fig. 5. Transversely cladded rail was found to be harder in the clad zone because of its dendritic martensitic microstructure whereas the hardness of the longitudinally cladded rail showed a small variation in three zones close to the virgin rail. In the HAZ of transversely deposited cladding, the higher hardness gradient can indicate higher residual stress.

World Academy of Science, Engineering and Technology
International Journal of Civil and Environmental Engineering
Vol:11, No:9, 2017

B. Residual Stress

Fig. 6 shows the residual stresses of virgin rail through thickness measured by neutron diffraction. The transverse residual stress component close to the top surface is found as compressive about 200±20 MPa. The zero-normal component was considered in this measurement. Tensile residual stresses gradually increase in every direction and at 3.5 mm below the surface; there is a maximum residual stress of 200±20 MPa in the transverse component. After laser cladding, a change in the longitudinal residual stress distribution was observed and higher compressive residual stresses were found in the cladding-substrate interface, as shown in Fig. 7. Following the laser cladding, higher longitudinal compressive residual stress at the top surface decreased rapidly towards the fusion line and turned into tensile stress. Highest compressive residual stress (460±20 MPa) at the clad surface was below the yield strength value of the material. Higher compressive residual stresses are known to be beneficial for wear and fatigue performances but because of the high value of compressive stress at the clad zone, there was balancing higher tensile residual stress at the deeper surface, which may influence crack propagation. On the cladded rail, tensile stresses were found in the HAZ but beneficial compressive stress was found below the fusion line.
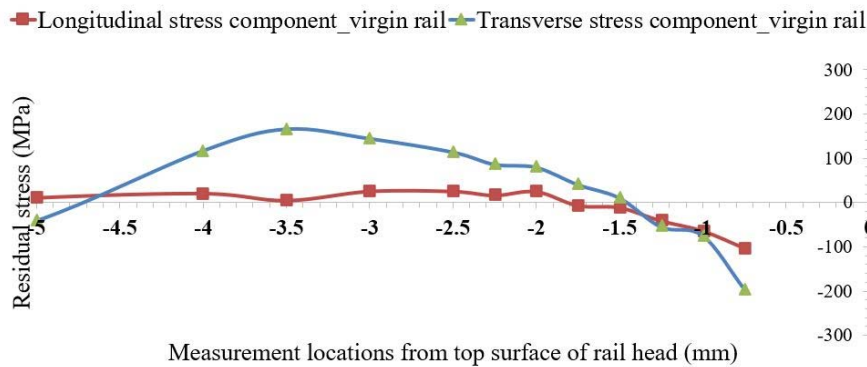

Fig. 6 The longitudinal and transverse components of residual stress for the virgin rail considering normal component as zero. X=0 represents the top surface of the rail
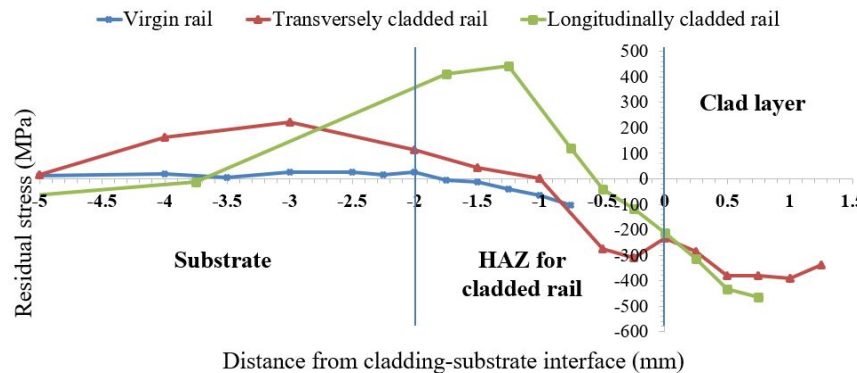

Fig. 7 Comparison of the longitudinal stress component of cladded and virgin rail; X=0 represents the diffusion line

IV. Conclusions

The key findings of this experimental study were:

- Dendritic ferritic microstructure formed in the cladding area during the transversely cladded railhead, which causes the higher hardness in the clad zone.
- Large hardness variation was found in cladding and substrate zone for transversely cladded railhead.
- Longitudinally cladded rail head achieved acceptable hardness values in the clad layer.
- Compressive residual stress was found at the top surface of the virgin and cladded rails.
- The laser cladding process introduced compressive stress value at the cladding surface and correspondingly tensile stress in the HAZ.

- For the cladded railhead, the tensile residual stress is higher but occurs deeper in the rail creating a small amount of beneficial compressive stress at the interface (fusion line)
- Based on this study; longitudinally cladded rail has revealed significantly better microstructure, hardness and residual stress profile through the thickness, as such it is the highly recommended direction for railhead repairs.

World Academy of Science, Engineering and Technology
International Journal of Civil and Environmental Engineering
Vol:11, No:9, 2017

REFERENCES

[1] F.C.R. Hernández, N.G. Demas, K. Gonzales, and A.A. Polycarpou, *Correlation between laboratory ball-on-disk and full-scale rail performance tests.* Wear, 2011. 270(7): p. 479-491.

[2] W. Hui, Z. Xu, Y. Zhang, X. Zhao, C. Shao, and Y. Weng, *Hydrogen embrittlement behavior of high strength rail steels: A comparison between pearlitic and bainitic microstructures.* Materials Science and Engineering: A, 2017. 704: p. 199-206.

[3] K.M. Lee and A.A. Polycarpou, *Wear of conventional pearlitic and improved bainitic rail steels.* Wear, 2005. 259(1): p. 391-399.

[4] F.C.R. Hernandez, N.G. Demas, D.D. Davis, A.A. Polycarpou, and L. Maal, *Mechanical properties and wear performance of premium rail steels.* Wear, 2007. 263(1): p. 766-772.

[5] D. Cannon, K.O. EDEL, S. Grassie, and K. Sawley, *Rail defects: an overview.* Fatigue & Fracture of Engineering Materials & Structures, 2003. 26(10): p. 865-886.

[6] I. Tabernero, A. Lamikiz, S. Martínez, E. Ukar, and J. Figueras, *Evaluation of the mechanical properties of Inconel 718 components built by laser cladding.* International Journal of Machine Tools and Manufacture, 2011. 51(6): p. 465-470.

[7] P. Webster, K. Low, G. Mills, and G. Webster, *Neutron measurement of residual stresses in a used railway rail.* MRS Online Proceedings Library Archive, 1989. 166.

[8] G. Webster, P. Webster, M. Bourke, K. Low, G. Mills, H. McGillivray, D. Cannon, and R. Allen, *Neutron diffraction determinations of residual stress patterns in railway rails.* Residual Stress in Rails, ibid, 1992: p. 143-152.

[9] P. Webster, G. Mills, X. Wang, and W. Kang, *Residual stress measurements in rails by neutron diffraction*, in *Rail Quality and Maintenance for Modern Railway Operation*. 1993, Springer. p. 307-314.

[10] V. Luzin, J.E. Gordon, T. Gnaupel-Herold, and H.J. Prask. *Neutron residual stress measurements on rail sections for different production conditions*. in *Proceedings of IMECE*. 2004. ASME Anaheim, CA.

[11] Z. Wen, X. Jin, and W. Zhang, *Contact-impact stress analysis of rail joint region using the dynamic finite element method.* Wear, 2005. 258(7): p. 1301-1309.

[12] 12. Q. Lai, R. Abrahams, W. Yan, C. Qiu, P. Mutton, A. Paradowska, and M. Soodi, *Investigation of a novel functionally graded material for the repair of premium hypereutectoid rails using laser cladding technology.* Composites Part B: Engineering, 2017.

[13] J.C. Ezechidelu and S.O. Enibe, *Effect of Heat Treatment on the Microstructure and Mechanical Properties of a Welded AISI 410 Martensitic Stainless Steel.*

[14] A. Rajasekhar, G.M. Reddy, T. Mohandas, and V. Murti, *Influence of austenitizing temperature on microstructure and mechanical properties of AISI 431 martensitic stainless steel electron beam welds.* Materials & Design, 2009. 30(5): p. 1612-1624.

[15] Access from: *http://www.thefabricator.com*. Access date: 8th September 2017